Article

Influence of Gas Inlet Slit Width on Gas-Assisted Plastic Micro-Tube Extrusion

Shuiquan Chen, Xingyuan Huang *, Bin Liu and Xiaohui Zhang

College of Advanced Manufacturing, Nanchang University, Nanchang 330031, China; chenshuiquan3@163.com (S.C.)

* Correspondence: xyhuang@ncu.edu.cn

Abstract: In the process of the double-layer gas-assisted extrusion of plastic micro-tubes, the external size and surface quality of the micro-tubes are greatly affected by the size of the assisting gas inlet slit inside the mold. Therefore, in this experiment, a two-phase flow model was established based on a compressible gas and a non-compressible melt. The Polyflow finite element solution software module was used to solve the velocity field, temperature field, pressure field, and section size of the melt under the condition of double-layer gas-assisted extrusion in a mold under different gas inlet slit widths. The results show that, with an increase in the width of the gas inlet slit, the melt outlet velocity increases, the surface temperature increases, wall thickness shrinkage increases, and interior diameter expansion increases. In the process of gas-assisted extrusion, the thickness of the air cushion is affected by adjusting the size of the gas inlet slit, and, hence, changes the shape and size of the plastic micro-tubes.

Keywords: gas-assisted extrusion; numerical simulation; gas–liquid two-phase model; extrusion deformation

1. Introduction

Plastic micro-tubes are widely used in medicine, telecommunications, automobiles, and other fields, with significant value added [1,2]. Nevertheless, owing to the viscoelastic properties of their materials, micro-tubes are susceptible to dimensional fluctuations throughout production. To enhance product excellence and minimize wastage, it is imperative to address the treatment methodology for polymer micro-tubes [3]. Die configuration is crucial for ensuring the quality of polymer tubes. Historically, numerous academics have undertaken extensive investigations into the optimal design of conventional extrusion molds for micro-scale polymer conduits [4–8]. Jin [9] conducted an experimental study on how the dimensions of polypropylene (PP) micro-tubes are influenced by the parameters of a micro-tube molding tool with a single cavity. The findings indicate that the molding tool dimensions have a significant impact on the micro-tube's diameter and wall width. Several studies have explored how the rheological properties of polymers are affected by the process parameters of micro-tube molding, and numerical simulations have been used to investigate the extrusion expansion phenomenon. Luo [10] studied the expansion memory phenomenon of polymer melts in the ring region. Yao [11] investigated the rheological properties of polymer materials during microchannel filling. Liu [12] studied the viscoelastic rheological properties of polymer melt during cross-scale extrusion. Wang [13] proposed a shear viscosity measurement method and viscosity model for polymer melt at the micro scale. Xiao [14] analyzed the flow characteristics of polymer micro-tube extrusion. Xiao [15] discussed the rheological properties of plastic polyurethanes. Zhao [16] studied the phenomenon of wall slip in the process of micro-extrusion flow. Wei [17] has carried out research on a multi-specification polylactic acid micro-tube extrusion process. Jin [18] conducted research on the two-cavity micro-tube extrusion process. Wang [19] studied the forming and process parameters of rectangular micro-tube extrusion. Deng [10,11] explored

the influence of the length of the micro-tube forming section on the processing. Neverthe-less, the conventional molding process for extrusion involves the elastic restoration of the melt in the die by wall shear, which may result in defects such as deformation, extrusion swelling, and melt cracking [20–23]. Although analysis of the traditional extrusion process can improve the quality of the extrusion product to a certain extent, it is still difficult to solve the above defects.

The application of gas-assisted techniques in the extrusion of plastic micro-tubes can effectively tackle these challenges by transforming the molten material within the die from a viscous flow to a slip flow regime [24–28]. Liang [29] introduced the slit inlet method, which utilizes gas-assisted technology to create a stable air cushion between the mold and the polymer melt, resulting in a significant reduction in die resistance. Ren [30,31] developed a numerical simulation for the extrusion of polymers using gas-assisted extrusion, which models the two-phase flow of gas and polymer melt. Both experimental and numerical findings demonstrate the impact of gas pressure on the contraction of the polymer melt morphology. Liu [32] explored the principle of gas layer formation and analyzed the effect of gas pressure on the effects of micro-tube molding.

Although the diameters and wall thicknesses of micro-tubes are small, high precision is required. In the double-layer gas-assisted extrusion model previously established by researchers, the initial position of the numerical simulation was set in the shaping section because it was assumed that the melt and gas were stable in the shaping section, ignoring the influence of the gas inlet slit. Figure 1 shows a three-dimensional model of the mouth die of a double-layer gas-assisted extrusion micro-tube set-up. The gas impacts at the interface between the inlet and the melt, making it difficult to form a stable air cushion here. The impact of the gas on the interface with the melt affects the size and surface quality of the micro-tube that forms. As a result, the current theoretical model is not accurate enough to predict melt formation. These problems restrict the growth of micro-tube extrusion processing technology. In order to better explore the factors influencing the micro-tube extrusion process, in this paper, we establish a gas–liquid two-phase flow geometry model of double-layer gas-assisted extrusion. The impact of gas inlet slit width on micro-tube formation is numerically simulated and experimentally verified. In this model, we propose that, before the initial position of the model is established in the gas auxiliary section, the impact of gas on the melt and pressure loss are taken into account to better explore the influence of these processes.
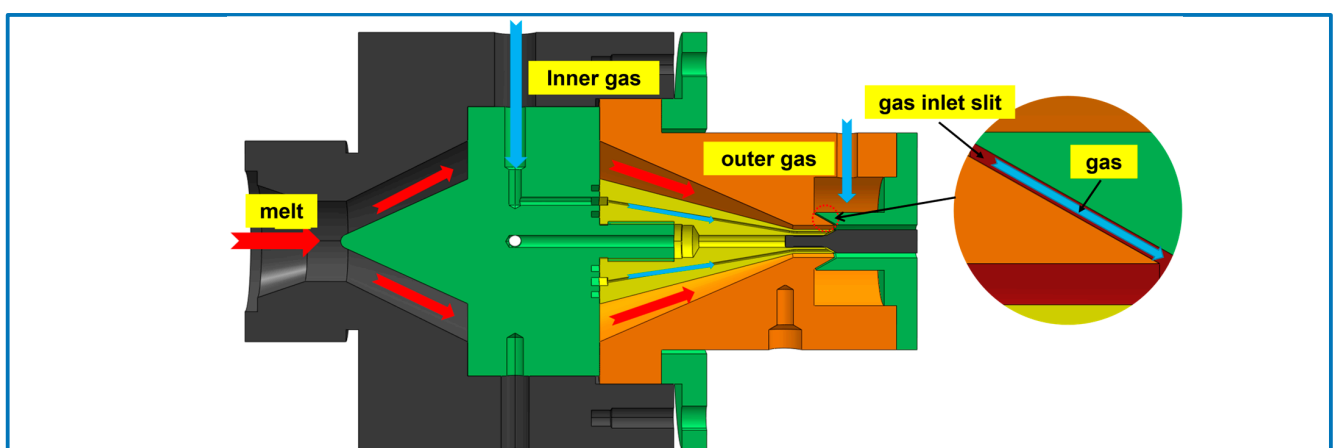

Figure 1. 3D model of a mouth die.

2. Numerical Simulation Theory and Model Setting

2.1. Control Equations and Constitutive Equations

The finite element simulation process makes use of the following assumptions: because of the high viscosity and low velocity of the polymer melt, the gas has a low viscosity and mass, and the inertial and gravitational effects of both fluids are negligible. The gas is

compressible and a Newtonian fluid, while the polymer melt is a non-Newtonian fluid and has poor compressibility, and is taken as incompressible [31]. The influences of surface tension, mutual penetration, and relative slippage between the gas and the melt are ignored. The melt and gas constitutive equations are simplified as follows:

Continuity equation:

$$\nabla \cdot (\rho_k v_k) = 0 \tag{1}$$

Momentum conservation equation:

$$\rho_k v_k \cdot \nabla v_k + \nabla \rho_k - \nabla \tau_k = 0 \tag{2}$$

Energy conservation equation:

$$\rho_k C_V \left(\frac{\partial T_k}{\partial_t} + v_k \cdot \nabla T_k \right) = -\nabla \cdot q_k - T_k \left(\frac{\partial p_k}{\nabla T} \right) (\nabla \cdot v_k) + \tau_k : \nabla v_k \tag{3}$$

The flow of polymer melt in the mouth mold is described by the PTT viscoelastic differential constitutive equation [33] as follows:

$$\tau_r = \tau_1 + \tau_2 \tag{4}$$

$$\tau_2 = 2\eta_{12} D \tag{5}$$

$$\eta_{1r} = \frac{\eta_{12}}{\eta_1} \tag{6}$$

$$\exp\left[\frac{\varepsilon \lambda}{(1 - \eta_{1r})\eta_1} tr(\tau_1) \right] + \lambda \left[(1 - \frac{\xi}{2}) \overset{\nabla}{\tau_1} + \frac{\xi}{2} \overset{\nabla}{\tau_1} \right] = 2(1 - \eta_{1r})\eta_1 D \tag{7}$$

The flow of auxiliary gas is described by the gas equation of state as follows:

$$P_1 = \rho_1 \cdot R \cdot T_1 \tag{8}$$

2.2. Geometric and Finite Element Models

Figure 2a shows the flow process of the polymer melt in the mold. In the process of gas-assisted extrusion of micro-tubes, there are interior and exterior gas layers in both the interior and exterior micro-tube walls of the mold and the gas in the interior and exterior gas layers enters through gaps to form an air cushion between the melt and the wall surface. Due to the axial symmetry of the plastic micro-tubes, the two-dimensional model diagram along the flow path shown in Figure 2b and the two-dimensional 1/2 axisymmetric method were used for the calculation. In this figure, ABEF represents the area of the melt inside the mold, EFHG represents the area of the melt outside the mold, IJCEOM represents the interior gas cushion area, KLNPFD represents the exterior gas cushion area, and the Y-axis represents the center axis of the micro-tube. The distance from the Y-axis to AE is 3 mm; The length of the melt before the melt intersects the gas, denoted by AC and BD, is 5 mm; the length of the interfaces between the melt and exterior gas and interior gas, denoted by CE and DF, is 30 mm; the length of the free surfaces, denoted by EG and FH, is 10 mm; the thickness of the melt, denoted by AB, is 1 mm. the width of the gas inlet slit, denoted by IJ and KL, is set at 5×10^{-5} m, 1×10^{-4} m, 2×10^{-4} m, or 5×10^{-4} m; and the thickness of the gas cushion layer, denoted by OE and FP, is 0.1 mm. In order to improve calculation accuracy and reduce calculation difficulty, the boundary grid method and bias setting needed to carry out mesh refinement processing were only applied to the parts with large changes in fluid motion state, including the inlet and outlet of the die. The final finite element model was constructed as shown in Figure 2c.
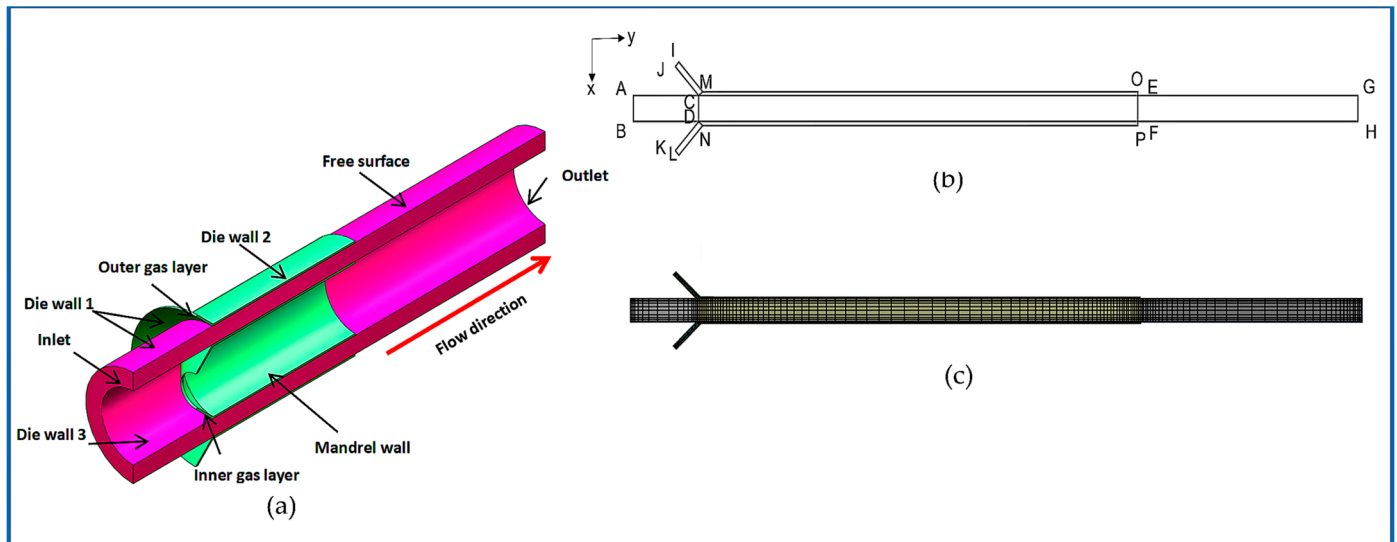
Figure 2. Geometric and mesh model, (**a**) 3D geometric model; (**b**) 2D geometric model; (**c**) mesh model.

2.3. Numerical Simulation Parameters

The equation parameters of the auxiliary gas and polypropylene (PP) are shown in Table 1. These represent the physical properties of the auxiliary gas and polypropylene melt at a reference temperature of 200 degrees Celsius and are taken from Liu [3].

Table 1. Numerical simulation parameters.

Equation Parameters	Melt	Gas
$\eta_1/(\text{Pa s})$	8823	2.6×10^{-5}
$\lambda/(\text{s})$	0.1	0
ε	0.15	0
ξ	0.44	0
η_{1r}	0.12	0
$q_k/(\text{W·m}^{-1}\text{·K}^{-1})$	0.22	0.037
$C_V/(\text{J·kg}^{-1}\text{·K}^{-1})$	1883	1026

2.4. Boundary Conditions Setting

AB is the melt inlet boundary. As the melt enters the forming section, it is assumed that the melt forms a fully developed non-Newtonian viscoelastic laminar flow. IJ and KL are gas inlet boundaries. ACJ, BDK, IMO, and LNP are wall boundaries. CE and DF are the interfaces between the gas and the melt. EG and FH are the free surface boundaries of the melt. GH is the melt outlet boundary. OE and FP are the gas outlet boundary. The boundary conditions include the flow boundary and the thermal boundary.

(1)　The flow boundary is set as follows:

AB was set as "inflow", volume flow rate was 1×10^{-8} m^3/s. IJ and KL are set as " $f_n = 5000$ Pa, $f_s = 0$ ". ACJ, BDK, IMO, and LNP are set as "Zero wall velocity ($v_n = v_s = 0$) ". CE and DF are set as "interfaces", and the interface is required not to penetrate, and there is no slip at the junction of the two-phase fluid. EG and FH are set as "free surface". GH was set as "$f_n = v_n = 0$", with no external traction. OE and FP are set as "$f_n = v_n = 0$", also without external traction.

(2)　The thermal boundary is set as follows:

AB, IJ, KL, ACJ, BDK, IMO, and LNP are set as "Temperatures along the boundary are 392 °F". CE and DF are set as "Interface". EG and FH are set as "Flux density imposed along boundary". GH, OE, and FP are set as "Outflow".

2.5. Numerical Simulation Method

ANSYS Workbench is a commonly used platform for solving finite element problems. The DesignModeler module is used to establish the geometric models and the meshing module is used for meshing. The POLYFLOW module is then used to set up a 2D axisymmetric calculation task and solve the finite element problem. Finally, the CFD-Post module is used for post-processing and exporting the calculation results for data processing and analysis. Because of the rheology of high-viscosity and high-elasticity polymer melt, the constitutive equation of the melt is nonlinear, and the calculation process does not easily converge. In order to make the solution of the equation converge better, the initial conditions of melt relaxation time and inlet velocity are set using the Evolution method. In order to improve solution accuracy and efficiency, the spine kinematics equation is used to reset the free-form surface boundary mesh. In addition, in the process of model solving, a variety of methods to promote the steady-state calculation of finite elements are comprehensively used, including the viscoelastic separation method for calculating the stress tensor and the uncoordinated streamline windward method.

3. Simulation Results and Analysis

The change in melt flow state in the mold will affect micro-tube size and surface quality. In the numerical simulation, by keeping the gas pressure and melt inlet parameters and boundary conditions unchanged, and changing the width of the slit inside and outside the gas auxiliary inlet, the influence law of the slit width of the gas-assisted inlet on the melt velocity field, pressure field, temperature field, interior diameter, and wall thickness was studied.

3.1. Micro-Tube Size Distribution

This section mainly evaluates the extent of the influence of gas inlet slit width on micro-tube size from two dimensions: interior wall radius and thickness. The rate of change of the interior diameter of the micro-tube is defined as: $C_R = \frac{R_N - R_1}{R_1} \times 100\%$ and the rate of change of the wall thickness of the guide tube is defined as: $C_T = \frac{T_N - T_1}{T_1} \times 100\%$. Where R_N and T_N are the truncation surface micro-tube radius and wall thickness, and R_1 and T_1 are the die exit tube radius and wall thickness, respectively. The calculation results are shown in Figure 3. Figure 3a shows the change in melt interior radius along the axial direction under the condition that other conditions remain unchanged and only the width of the inlet slit is changed. Figure 3b shows the change in micro-tube wall thickness along the axial direction. Figure 3c shows the relationship between the rate of change of the micro-tube interior diameter and wall thickness and the change of the width W of the inlet slit.

As can be seen from Figure 3a,c, the micro-tube interior diameter tends to increase with an increase in the distance from the left end face of the gas-assisted section of the mouth mold, while the micro-tube interior diameter near the exit of the mouth mold tends to be stable. The expansion rate of the interior diameter increases with an increase in the width W of the gas inlet slit, and the rate of this increase shows a nonlinear trend from fast to slow. It can be seen from the data in Figure 3b,c that the micro-tube wall thickness tends to decrease with an increase in the distance from the left end face of the gas-assisted section, while the micro-tube wall thickness tends to be stable near the die outlet, and the shrinkage rate of the micro-tube wall thickness increases with an increase in the width W of the gas inlet slit. This is because the increase in the width of the gas inlet slit leads to a larger amount of gas flowing into the air cushion, which results in the gas squeezing the melt space in the mouth mold.
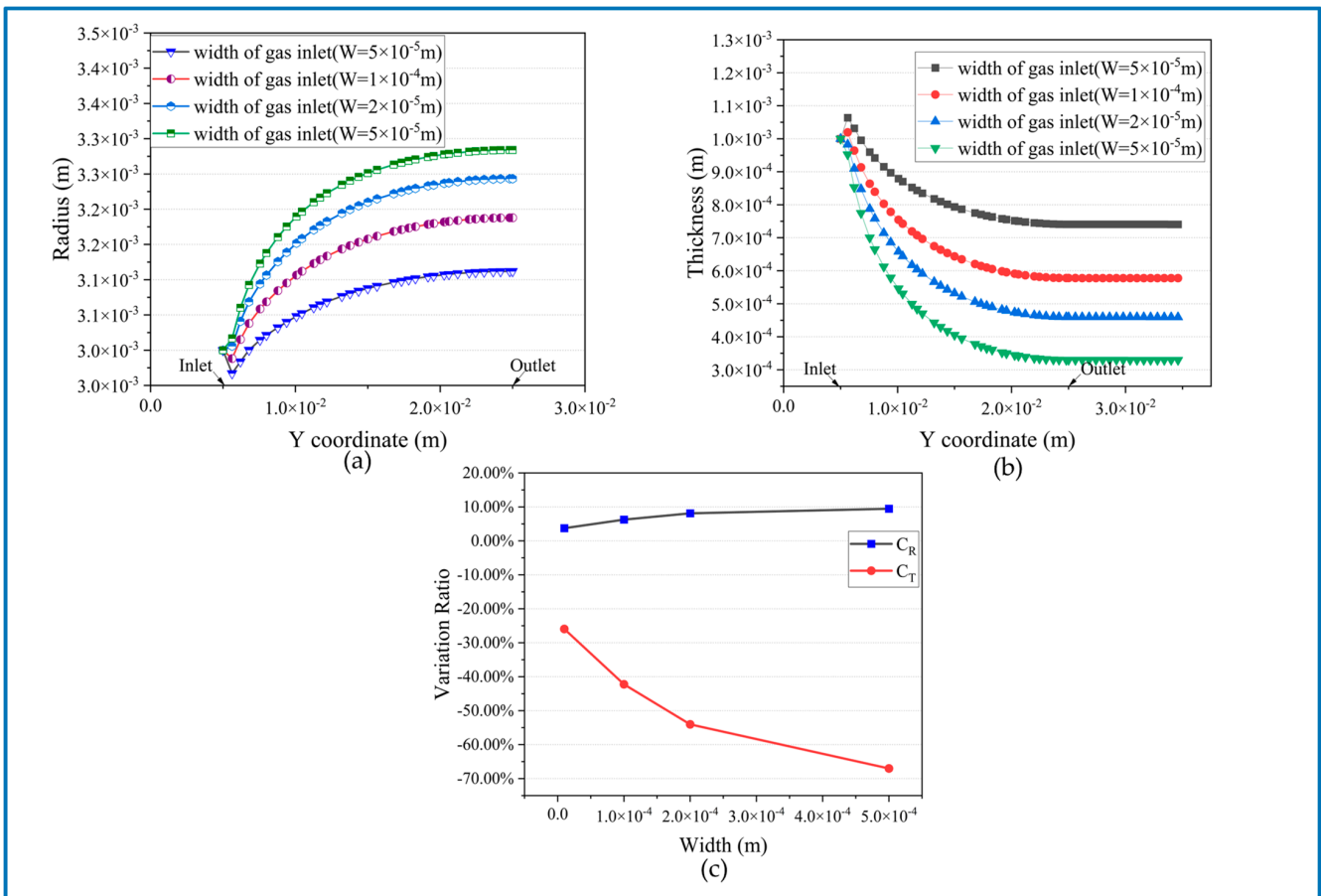
Figure 3. The wall thickness and exterior wall radius of a micro-tube along the Y-axis under different gas inlet slit widths and the rate of change of micro-tube thickness and exterior diameter at the outlet under different gas inlet slit widths. (**a**) Wall thickness of the micro-tube; (**b**) the exterior wall radius of the micro-tube; and (**c**) rate of change of thickness and outside diameter.

3.2. Velocity Field Distribution

Figure 4 shows the velocity distribution cloud diagram along the Y direction of the interface between the melt in the micro-tube and the gas layer in the wall. Under the condition that other conditions remain unchanged, when the width of the gas inlet slit W is constant, the velocity component in the Y direction of the interface surface between the melt and the air increases with an increase in the distance from the left end face of the gas auxiliary section of the die. The velocity in the Y direction tends to be stable until it approaches the outlet of the die, and the velocity in the Y direction of the final outlet increases with an increase in the gas inlet slit. Figure 5 shows the changes in the velocity components of the interior and exterior walls of the melt along the Y-axis direction under different inlet slit widths. The continuous increase in melt velocity is due to the drag effect of the gas on the melt. The reason why the melt velocity increases with an increase in the width of the gas inlet slit is as follows: As the width of the gas inlet slit increases, the volume of gas entering the air cushion increases, which compresses the melt space. Under the condition that the flow rate at the melt inlet is constant, the flow rate at the outlet is the same. Thus, the smaller the compressed space of the melt, the faster the velocity at the interface.
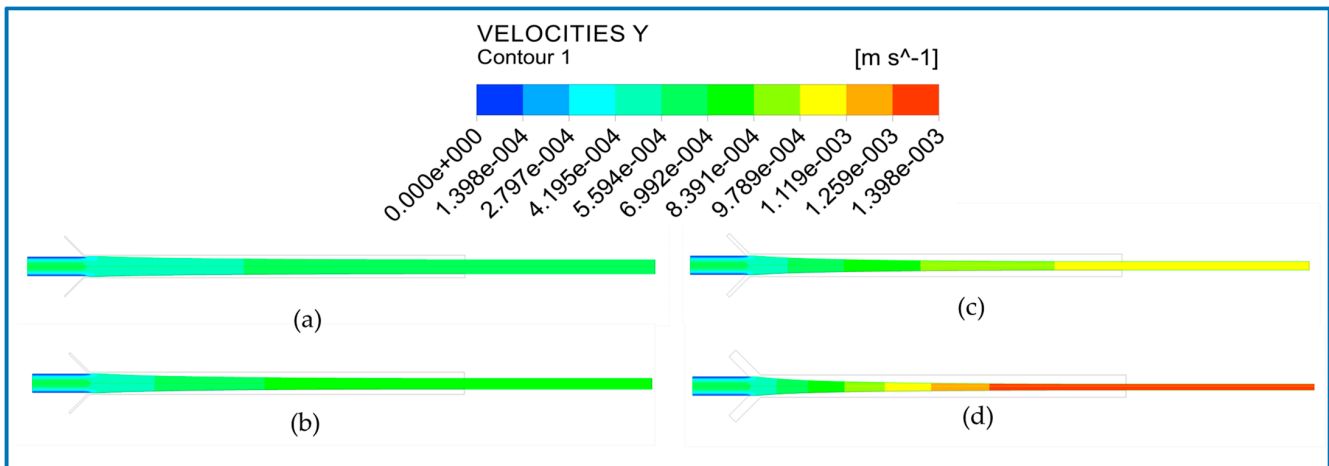
Figure 4. Cloud diagram of velocity components along the Y-axis of the melt with different gas inlet slit widths. (**a**) W = 5.0×10^{-5} m; (**b**) W = 1.0×10^{-4} m; (**c**) W = 2.0×10^{-4} m; (**d**) W = 5.0×10^{-4} m.
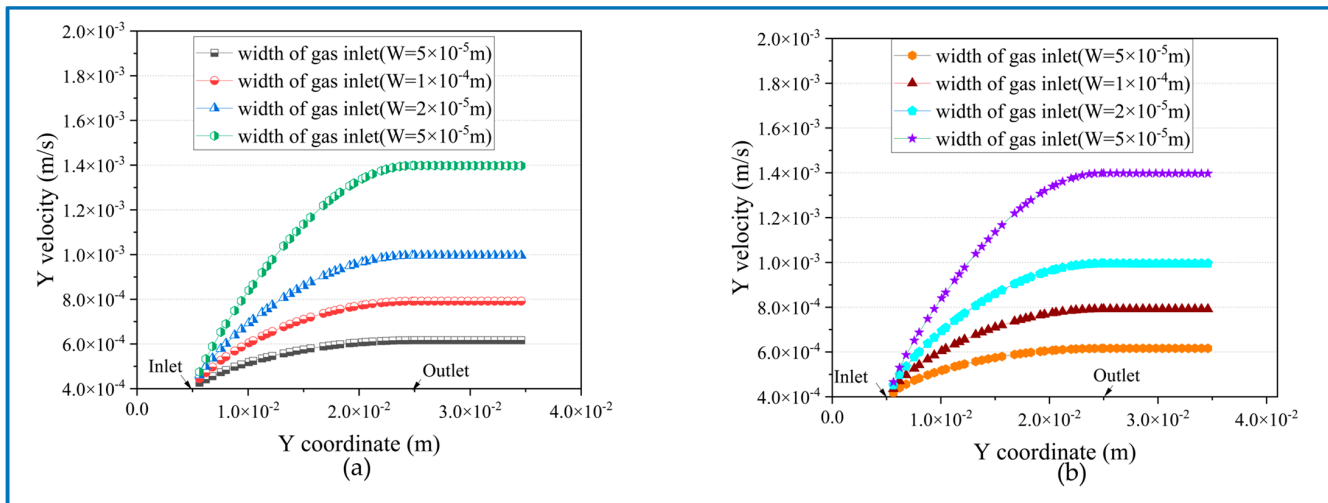

Figure 5. The variation in velocity components along the Y-axis on the interior and exterior walls of melt under different gas inlet slit widths. (**a**) Interior wall velocity variation; and (**b**) exterior wall velocity variation.

3.3. Distribution of Shear Rate

As shown in Figure 6, whether inside or outside the mold, at the interface between the gas and melt, the gas has a significant shearing effect on the melt wall, and the closer it is to the melt wall, the more obvious the shearing effect of the gas on the melt. The shear rate of both the interior and exterior interfaces of the melt increases sharply to a maximum value at the contact point of the gas and melt, then immediately decreases; while it tends to a stable value in the gas-assisted section, and decreases to 0 at the mouth model outlet.

With an increase in the width of the gas inlet slit, the melt surface shear rate increases. With other conditions unchanged, the shear rate of the exterior surface of the melt is higher than that of the interior surface of the melt at the same Y-axis coordinate, which indicates that the exterior gas cushion has a more obvious shear effect on the melt under the same gas inlet slit width and gas pressure. The shear action of the gas on the melt outside the die disappears because the compressed gas flow quickly flows into the air after the exit of the die and the loss of pressure no longer produces a drag effect on the melt, thus no longer having a shear action on the melt.
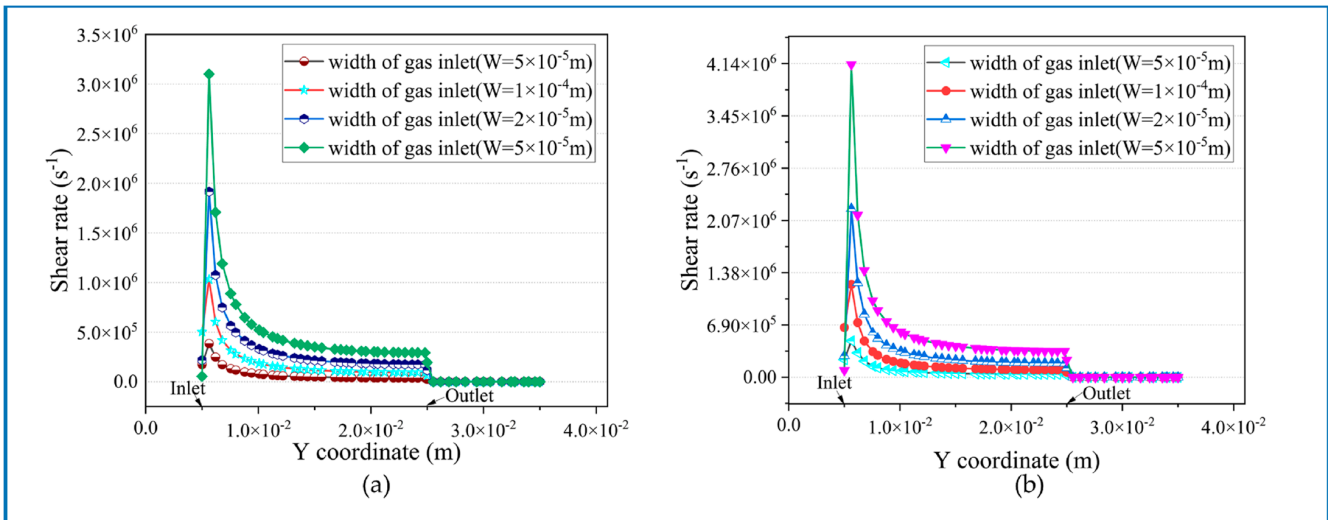
Figure 6. The shear rate of melt interior and exterior walls varies under different gas inlet slit widths. (**a**) Shear rate of the interior wall; and (**b**) shear rate of the exterior wall.

3.4. Pressure Field Distribution

Figure 7 shows the pressure field distribution of the melt under different slit widths of the gas inlet.
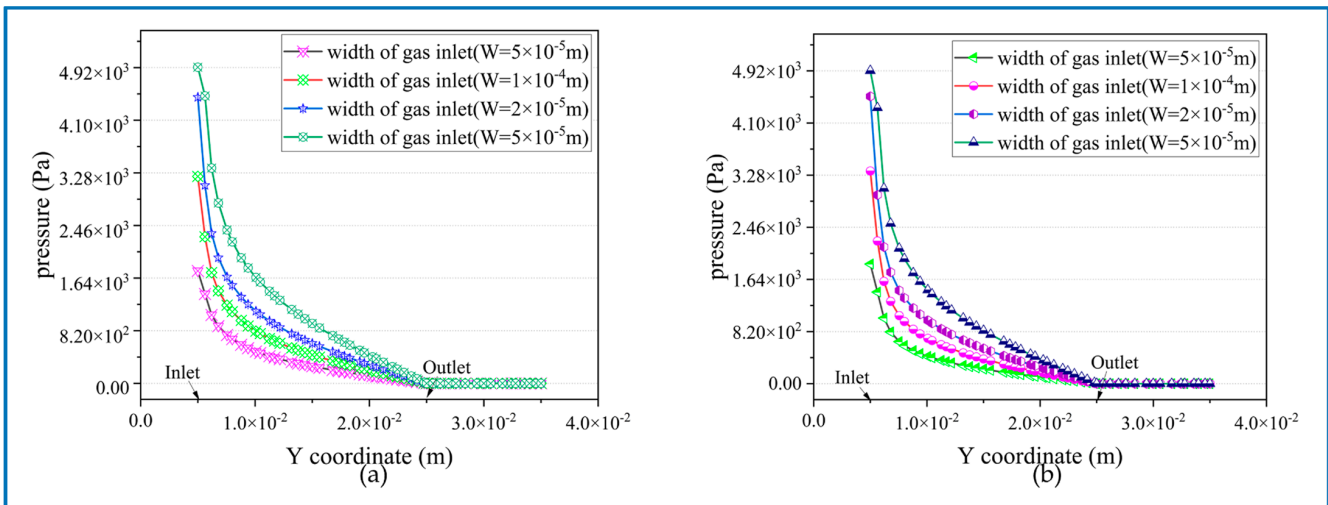

Figure 7. Pressure field distribution of melt under different gas inlet slit widths. (**a**) Pressure distribution of interior melt wall; and (**b**) pressure distribution of exterior melt wall.

As shown in Figure 7, the melt generates a large pressure drop in the gas-assisted section until the pressure drops to 0 at the die outlet. The pressure drop in the gas-assisted section presents a nonlinear relationship, and with an increase in the width of the gas inlet slit, the pressure increases along the same Y-axis direction. When the gas inlet pressure is set to 5000 Pa, as the width of the gas inlet slit decreases, the pressure at the starting point of the gas and melt interface decreases, because the friction between the gas and the wall at the slit leads to the pressure drop. In addition, there is a pressure difference between the interior and exterior walls of the melt, which increases with an increase in the width of the gas inlet slit, which also leads to a deviation in the actual micro-tube wall center from the ideal micro-tube wall center. Meanwhile, the normal pressure difference between the interior and exterior surfaces of the melt is also the reason for the rearranging of the velocity field, stress field, and temperature field inside the melt.

3.5. Temperature Field Distribution

The temperature at the interface between the melt and the exterior gas cushion along the axial direction of the model, that is, the temperature on the exterior wall of the melt, is shown in Figure 8a. The temperature of the exterior wall of the melt increases rapidly when the melt contacts with the compressed assisting gas, and then tends to be stable. At the beginning of the gas-assisted section, the melt temperature rises sharply, mainly because the gas inlet is at an angle of 45°, and the gas has a velocity component perpendicular to the melt flow direction, which impacts the melt surface. At the outlet of the mold, the extrusion and shearing effect of the gas on the melt disappears because the gas flows into the air, the melt enters the air at normal temperature, and the temperature of the exterior wall decreases rapidly. As the width of the gas inlet slit W increases, the temperature of the melt increases, which is mainly due to the dominant effect of gas squeezing the melt. As can be seen from Figure 8d,e, in the same axial direction as the gas-assisted section, the melt temperature decreases with a decrease in the radius. This is because there is a difference in area between the exterior surface and the interior surface, and the pressure on the upper surface is greater than that on the lower surface.
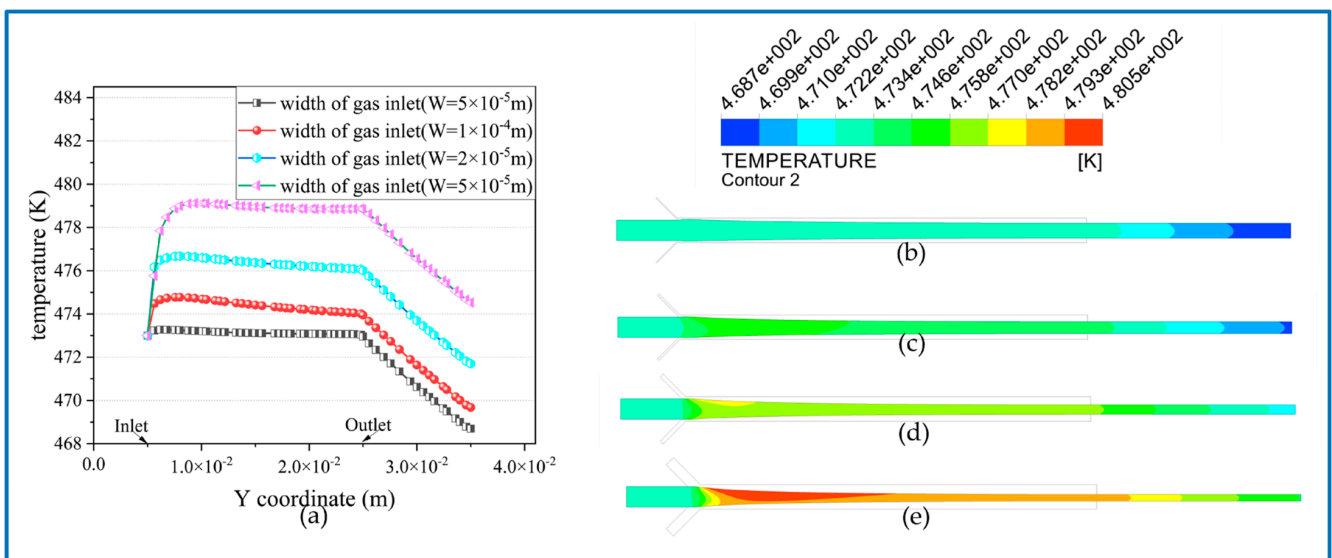

Figure 8. Temperature variation of melt exterior wall and temperature nephogram of melt interior under different gas inlet slit widths. (**a**) Melt exterior wall; (**b**) $W = 5.0 \times 10^{-5}$ m; (**c**) $W = 1.0 \times 10^{-4}$ m; (**d**) $W = 2.0 \times 10^{-4}$ m; and (**e**) $W = 5.0 \times 10^{-4}$ m.

4. Experimental Section

As shown in Figure 9, a double-layer gas-assisted extrusion experimental platform was established to verify the influence of the slit width of the gas-assisted inlet on plastic micro-tube extrusion. This experimental platform is the same as the equipment used in the experiment of Liu [3]. In order to ensure that the pressure and temperature of the internal and external air cushion remain consistent during the experiment, the double branch of the gas thermal control system is changed into a single branch, and finally divided into two paths to enter the mold.
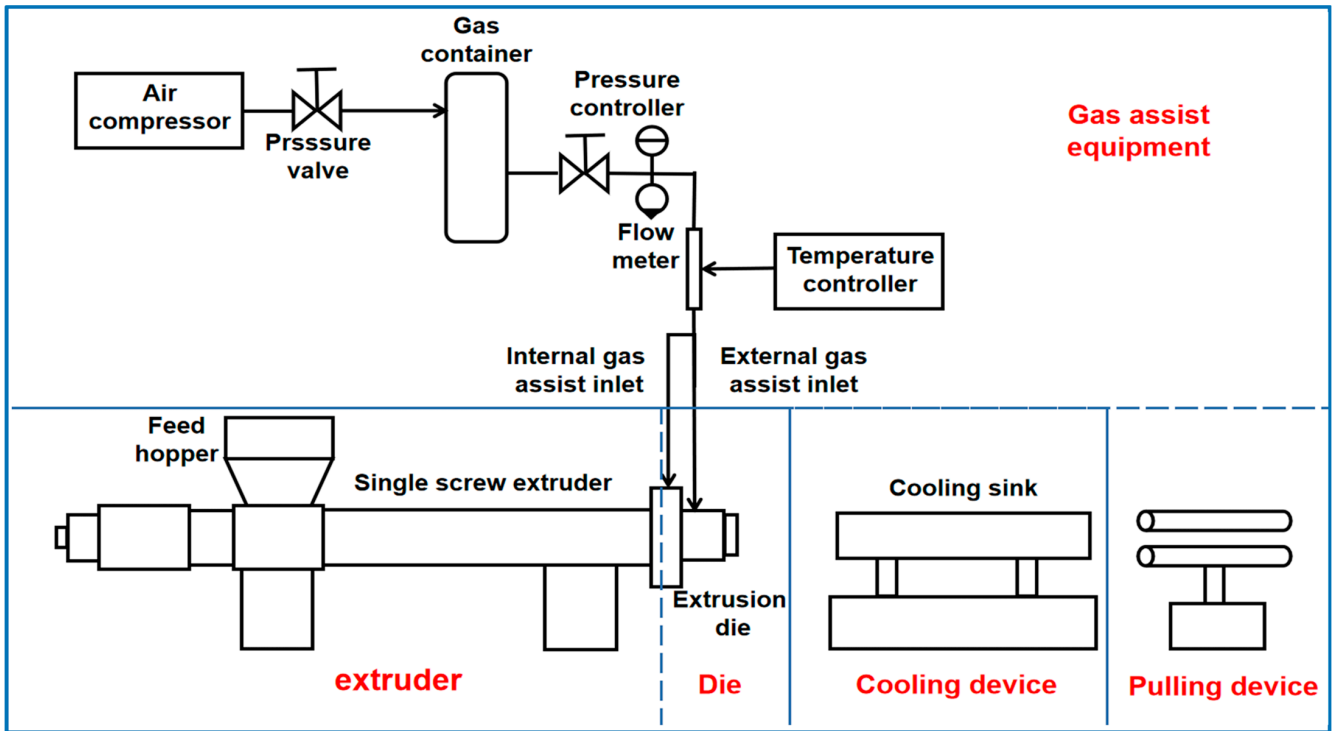
Figure 9. Schematic diagram of double-layer gas-assisted extrusion experimental platform.

Figure 10 shows the schematic diagram of the double-layer gas-assisted extrusion mold, which was independently designed by the laboratory team and is the most important component in the double-layer gas-assisted extrusion experimental equipment. The width of the slit of the exterior auxiliary gas inlet can be adjusted by using the adjusting screw, and the width of the slit of the interior auxiliary gas inlet can be adjusted by adjusting the die head.
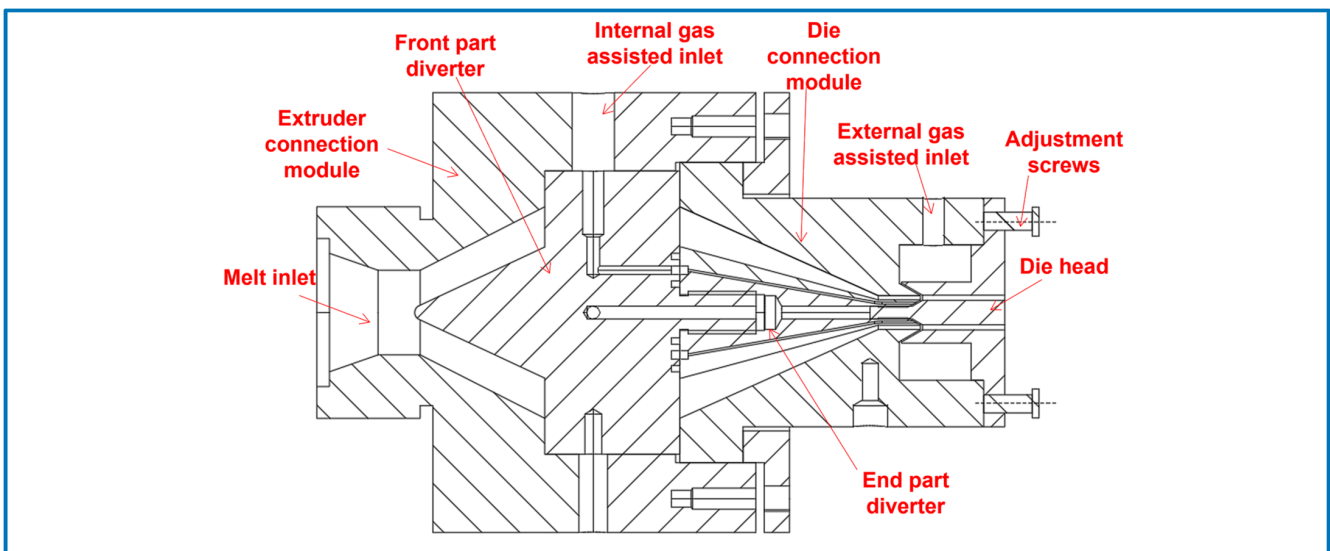

Figure 10. Schematic diagram of double-layer gas-assisted extrusion die.

Table 2 shows the experimental conditions.

Table 2. Experimental conditions.

Experiment Condition	Gas-Assisted Extrusion
Gas pressure/(Pa)	5000
Traction device frequency/(Hz)	4
Temperature of the die/(°C)	200
Extruder motor frequency/(Hz)	4
Gas inlet slit width (mm)	0.05/0.1/0.2/0.5

As shown in Figure 11 and Table 3, when the auxiliary gas inlet slit W = 5×10^{-4} m, there is obvious extrusion expansion at the abrasive tool outlet. This is because the gas inlet slit is too thin, which results in the gas not being able to form a stable and complete air cushion on the double wall of the melt. The phenomenon of the diameter decreasing after extrusion expansion is caused by the supporting action of the traction device, which makes the axial velocity at the outlet of the mold smaller than the traction velocity. The expansion phenomenon is not visible in the subsequent Figure 11b,c, because a stable and complete air cushion was formed in these experiments, and the gas at the air cushion had a certain dragging effect on the melt such that the exit speed approached or exceeded the traction speed of the traction device. In Figure 11d, the micro-tube is seen to expand at the mold outlet because the gas pressure drop decreases as the gas inlet slit increases and the gas entering inside and outside the gas layer increases. At the outlet of the mold, the gas pressure is still large, and the outer gas directly enters the air, while the inner gas is not quickly discharged, resulting in the pressure difference between the inner and outer walls of the micro-tube and the phenomenon of extrusion swelling. From the experimental data in Table 3, it can be seen that there are differences between the numerical simulation results and the experimental results, but the general trend of the experimental results is largely consistent with the simulation results. It can be seen that the micro-tube radius at the die outlet decreases significantly with an increase in the auxiliary gas inlet slit, which is largely consistent with the trend obtained by numerical simulation.

Table 3. Results of the extrusion experiment.

Gas Inlet Slit Width/W	Diameter (mm)	Wall Thickness (mm)
5×10^{-5} m	8.12	0.77
1×10^{-4} m	7.76	0.62
2×10^{-4} m	7.45	0.50
5×10^{-4} m	7.84	0.38

The obtained plastic micro-tubes were divided into several sections, and the wall thickness and outside diameter of each section were measured to obtain an average value. The following table shows the results of the extrusion experiment.
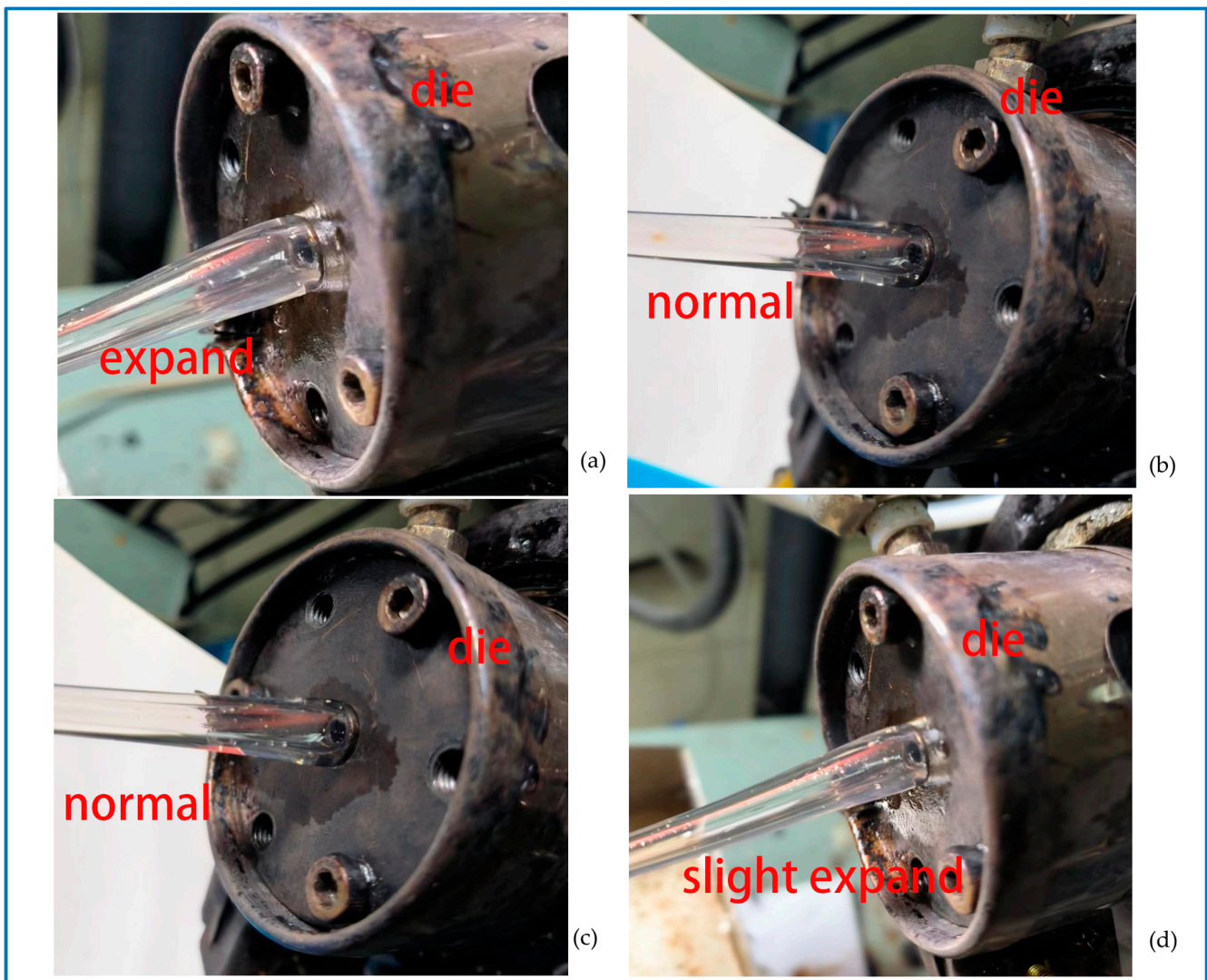
Figure 11. Experimental results of micro-tube extrusion. (**a**) W = 5×10^{-5} m; (**b**) W = 1×10^{-4} m; (**c**) W = 2×10^{-4} m; (**d**) W = 5×10^{-4} m.

5. Conclusions

The numerical simulation results show that the size of the auxiliary gas inlet slit has a great influence on the size and exit rate of extruded plastic micro-tubes. The expansion rate of the micro-tube diameter increases from 2.8% to 10% and the shrinkage rate of the micro-tube wall thickness increases from 25% to 67% with an increase in the gas inlet slit width.

The expansion in interior diameter expansion and contraction in wall thickness of the micro-tube are due to the increasing shear rate of the melt wall. This is mainly because, with the widening of the gas inlet slit, the thickness of the air cushion on the interior and exterior walls of the melt increases, which compacts the melt space. When the flow rate at the melt inlet remains unchanged, the melt outlet velocity increases and the melt is stretched.

In the process of gas-assisted extrusion, the size and output speed of the formed micro-tube can be adjusted to a certain extent by adjusting the width of the air inlet slit without changing the mold. By increasing the width of the inlet slit, the pressure loss of the gas in the slit can be reduced to a certain extent. Experiments show that, when the width of the slit at the gas inlet is below a certain value (between 0.05 mm and 0.1 mm), it is difficult to form a stable and complete air cushion in the gas auxiliary section, and extrusion swelling occurs.

Nomenclature

∇	Hamiltonian
ρ_k	density
ν_k	velocity vector
p_k	pressure
τ_k	bias stress tensor
C_V	specific heat capacity
T_k	temperature
q_k	thermal conductivity
$\tau_k : \nabla\nu_k$	viscous dissipation term
τ_r	melt stress tensor
τ_1	elastic component of the melt bias stress tensor
τ_2	viscous component of the melt bias stress tensor
η_{12}	Newtonian viscosity component of the melt
η_1	total viscosity of the melt
η_{1r}	viscosity ratio of the melt
λ	relaxation time
ε	material intrinsic parameter for the tensile properties of the melt
ξ	material intrinsic parameter for the shear properties of the melt
D	deformation rate tensor
P_1	gas pressure
ρ_1	gas density
T_1	gas temperature
R	gas constant ($R = 287$ $(\text{J}\cdot\text{kg}^{-1}\cdot\text{K}^{-1})$)
f_n	normal stresses on boundary surface
f_s	tangential stresses on boundary surface
v_R	normal velocities at the boundary surface
v_Z	tangential velocities at the boundary surface
W	width of the gas inlet slit

References

1. Liu, T.K.; Huang, X.Y.; Liu, H.S.; Ren, Z.; Luo, C.; Wang, D.Y. Effect of air on interior air cushion of plastic microtube gas assisted extrusion. *Polym. Mater. Sci. Eng.* **2020**, *36*, 75–86.
2. Ren, Z.; Huang, X.Y.; Liu, H.S. Influence of gas in interior air cushion layer in gas-assisted extrusion of plastic micropipes. *Mater. Guide* **2020**, *34*, 20193–20198.
3. Liu, B.; Huang, X.; Ren, S.; Luo, C. Effect of Pressure Difference between interior and exterior Gas Layer on Micro-Tube Deformation during Gas-Assisted Extrusion. *Polymers* **2022**, *14*, 3559. [CrossRef] [PubMed]
4. Jin, G.B.; Zhao, D.Y.; Wang, M.J.; Jin, Y.F.; Tian, H.Q.; Zhang, J. Study on design and experiments of extrusion die for polypropylene single-lumen micro tubes. *Microsyst. Technol.* **2015**, *21*, 2495–2503. [CrossRef]
5. Tang, D.; Fang, W.L.; Fan, X.H.; Li, D.Y.; Peng, Y.H. Effect of die design in microchannel tube extrusion. *Procedia Eng.* **2014**, *81*, 628–633. [CrossRef]
6. Jin, G.B. Research on Design and Manufacturing Technology and Extrusion Process of Polymer Micro-Extrusion Die for Interventional Medical Catheters. Ph.D. Thesis, Dalian University of Technology, Dalian, China, 2013.
7. Zhu, C.W.; Wu, D.M. The design of the die for Multi-lumen precision medical catheter. *Plastics* **2008**, *37*, 99–102.
8. Chen, X. The Research of Technology and Die in Continuous Extrusion of Microcellular Plastics. Ph.D. Thesis, Nanchang University, Nanchang, China, 2014.

9. Zhang, H.G.; Lamnawar, K.; Maazouz, A.; Maia, J.M. A nonlinear shear and elongation rheological study of interfacial failure in compatible bilayer systems. *J. Rheol.* **2016**, *60*, 1–23. [CrossRef]

10. Luo, X.L.; Mitsoulis, E. Memory phenomena in extrudate swell simulations for annular dies. *J. Rheol.* **1989**, *33*, 1307–1327. [CrossRef]

11. Yao, D.; Kim, B. Simulation of the filling process in micro channels for polymeric materials. *J. Micromech. Microeng.* **2002**, *12*, 604–610. [CrossRef]

12. Liu, K.; Wang, M.J.; Zhao, D.Y.; Li, H.X. Viscoelastic rheological properties of polymer melts in cross-scale extrusion processes. *China Mech. Eng.* **2021**, *32*, 1494–1503.

13. Wang, M.J.; Tian, H.Q.; Zhao, D.Y. Micro-scale shear viscosity testing approach and viscosity model of polymer melts. *J. Mech. Eng.* **2012**, *48*, 21–29. [CrossRef]

14. Xiao, X.H. Analysis and Experimental Study of Polymer Micro Tubing Extrusion Flow. Ph.D. Thesis, Central South University, Changsha, China, 2013.

15. Xiao, J.H.; Chen, S.W. Rheological properties of medical grade thermoplastic polyurethane. *Polym. Mater. Sci. Eng.* **2016**, *32*, 87–90.

16. Zhao, D.Y.; Wang, M.J.; Song, M. Experimental study and molecular dynamics simulation of wall slip in a micro-extrusion flowing process. *Mech. Eng. Sci.* **2012**, *225*, 1175–1190. [CrossRef]

17. Wei, Y.B.; Wang, M.J.; Zhao, D.Y.; Liu, K.; Shen, Z.N. Study on single-die multi-specification polylactic acid microtube extrusion molding process. *Polym. Mater. Sci. Eng.* **2019**, *35*, 95–102.

18. Jin, G.B.; Wang, M.J.; Zhao, D.Y.; Tian, H.Q. Experimental investigation of extrusion process of double-lumen micro tube. *J. Mech. Eng.* **2012**, *48*, 19–27. [CrossRef]

19. Wang, L. Study on Extrusion Molding and Processing Parameters of Polymeric Microtubes with Rectangular Microchannels. Ph.D. Thesis, Zhejiang University, Hangzhou, China, 2020.

20. Mu, Y.; Zhao, G.Q.; Wu, X.G.; Zhai, J.Q. Finite-Element Simulation of Polymer Flow and Extrudate Swell Through Hollow Profile Extrusion Die with the Multimode Differential Viscoelastic Model. *Adv. Polym. Technol.* **2013**, *32*, 1–19. [CrossRef]

21. Zhao, L.Z. Research Progress in Extrusion Swell of Polymer Melt. *China Plast.* **2007**, *21*, 1–5.

22. Mu, Y.; Zhao, G.Q.; Zhang, C.R. Numerical Investigation of Viscoelastic Flow and Swell Behaviors of Polymer Melts in the Hollow Profile Extrusion Process. *Adv. Mater. Res.* **2010**, *97*, 209–213. [CrossRef]

23. Xu, X.M.; Zhao, G.Q.; Qin, S.X.; Wang, W.W. Numerical Simulation of Viscoelastic Extrudate Swell Through Elliptical Ring Die. *Chin. J. Chem. Eng.* **2011**, *19*, 10–17. [CrossRef]

24. Ren, Z.; Huang, X.Y.; Xiong, Z.H. Experimental and numerical studies for the gas-assisted extrusion forming of polypropylene micro-tube. *Int. J. Mater. Form.* **2020**, *13*, 235–256. [CrossRef]

25. Yin, H.N.; Huang, X.Y.; Liu, T.K.; Song, M.J. Effects of gas-assisted extrusion on slip in the cable coating process. *J. Polym. Eng.* **2021**, *41*, 329–337. [CrossRef]

26. Huang, X.Y.; Liu, H.S.; Zhou, G.F.; Luo, Z.M.; Li, S.Y. The Experimental Study of Air-Assisted Extrusion of Polymer. *China Plasitics* **2005**, *19*, 17–19.

27. Luo, C.; Huang, X.Y.; Liu, T.K.; Liu, H.S. Research on interior Gas Inflation Improvements in Double-layer Gas-assisted Extrusion of Micro-tubes. *Polymers* **2020**, *12*, 899. [CrossRef]

28. Huang, C.Y.; Liu, H.S.; Huang, X.Y.; Wan, Q.F.; Ren, Z. Numerical Simulation of Gas-assisted Extrusion Process of Microtube. *China Plast. Ind.* **2015**, *43*, 44–48.

29. Liang, R.F.; Mackley, M.R. The gas-assisted extrusion of molten polyethylene. *J. Rheol.* **2001**, *45*, 211–226. [CrossRef]

30. Ren, Z.; Huang, X.Y.; Liu, H.S.; Deng, X.Z.; He, J.T. Non-isothermal viscoelastic numerical analysis of compressible gas-assisted polymer extrusion molding. *CIESC J.* **2015**, *66*, 1615–1623.

31. Ren, Z.; Huang, X.Y.; Liu, H.S.; Deng, X.Z.; He, J.T. Numerical and experimental studies for gas assisted extrusion forming of molten polypropylene. *J. Appl. Polym. Sci.* **2015**, *132*, 1–13. [CrossRef]

32. Liu, T.K.; Huang, X.Y.; Luo, C.; Wang, D.Y. The Formation Mechanism of the Double Gas Layer in Gas-Assisted Extrusion and Its Influence on Plastic Micro-Tube Formation. *Polymers* **2020**, *12*, 355. [CrossRef]

33. Phan, T.; Tanner, R. A new constitutive equation derived from network theory. *J. Non-Newton. Fluid Mech.* **1977**, *2*, 353–365.